PII: S 0 3 0 9 - 1 7 0 8 (9 8) 0 0 0 2 7 - X

Analytical solutions for solute transport in saturated porous media with semi-infinite or finite thickness

Youn Sim & Constantinos V. Chrysikopoulos*

Department of Civil and Environmental Engineering, University of California, Irvine, CA 92697, USA

Three-dimensional analytical solutions for solute transport in saturated, homogeneous porous media are developed. The models account for three-dimensional dispersion in a uniform flow field, first-order decay of aqueous phase and sorbed solutes with different decay rates, and nonequilibrium solute sorption onto the solid matrix of the porous formation. The governing solute transport equations are solved analytically by employing Laplace, Fourier and finite Fourier cosine transform techniques. Porous media with either semi-infinite or finite thickness are considered. Furthermore, continuous as well as periodic source loadings from either a point or an elliptic source geometry are examined. The effect of aquifer boundary conditions as well as the source geometry on solute transport in subsurface porous formations is investigated. © 1999 Elsevier Science Ltd. All rights reserved.

Keywords: solute transport, analytical solution, multidimensional systems, nonequilibrium sorption, first-order decay.

NOMENCLATURE

a semi-axis of the elliptic source parallel to the x-axis [L]

a_1, a_2 defined in eqns (22) and (23), respectively

$\mathcal{A}$ defined in eqn (5)

b semi-axis of the elliptic source parallel to the y-axis [L]

$\mathcal{B}$ defined in eqn (6)

C solute concentration in suspension (liquid phase) [M L^{-3}]

C_0 source concentration [M L^{-3}]

C^* sorbed solute concentration (solute mass/solids mass) [M M^{-1}]

C_∞ steady-state solute concentration in the absence of decay [M L^{-3}]

D_x longitudinal hydrodynamic dispersion coefficient [L^2 t^{-1}]

D_y lateral hydrodynamic dispersion coefficient [L^2 t^{-1}]

D_z vertical hydrodynamic dispersion coefficient [L^2 t^{-1}]

erf[x]   error function, equal to $(2/\pi^{1/2}) \int_0^x e^{-z^2}\, dz$

E defined in eqn (B2)

$\mathcal{E}$ defined in eqn (A2)

f, f_0, f_1, f_2 arbitrary functions

F general functional form of virus source configuration [M L^{-3} t^{-1}]

*Corresponding author. E-mail: costas@eng.uci.edu

$\mathcal{F}^{-1}$	Fourier inverse operator
$\mathcal{F}_{\mathrm{fc}}$	finite Fourier cosine transform operator
$\mathcal{F}_{\mathrm{fc}}^{-1}$	finite Fourier cosine inverse operator
g	defined in eqn (B9)
G	source loading function [M t^{-1} (point source); M L^{-2} t^{-1} (elliptic source)]
H	finite aquifer thickness [L]
$\mathcal{H}$	defined in eqn (7)
$I_0[\cdot]$	modified Bessel function of first kind of order zero
$I_1[\cdot]$	modified Bessel function of first kind of first order
$K_0[\cdot]$	modified Bessel function of second kind of order zero
l_{x0}, l_{y0}, l_{z0}	x, y and z Cartesian coordinates, respectively, of a point source or the center of an elliptic source [L]
$\mathcal{L}^{-1}$	Laplace inverse operator
m	integer summation index
p	dummy integration variable
$\mathcal{P}$	defined in eqn (A27)
q	dummy integration variable
$\mathcal{Q}$	defined in eqn (A17)
r	radius of circular source [L]
r_1	forward rate coefficient [t^{-1}]
r_2	reverse rate coefficient [t^{-1}]
s	Laplace transform variable with respect to time
$\mathcal{S}$	defined in eqn (B7)
t	time [t]
U	average interstitial velocity [L t^{-1}]
v	dummy integration variable
W	source geometry function [L^{-3}]
x,y,z	spatial coordinates [L]

Greek symbols

α	arbitrary constant
α_x	longitudinal dispersivity [L]
α_y	lateral dispersivity [L]
α_z	vertical dispersivity [L]
β, β_1, β_2	arbitrary constants
γ	Fourier transform variable with respect to spatial coordinate x
$\delta(\cdot)$	Dirac delta function
ζ	dummy integration variable
η	defined in eqn (A23)
θ	porosity (liquid volume/porous medium volume) [L^3 L^{-3}]
$\kappa, \kappa_1, \kappa_2$	defined in eqns (26a), (24) and (25), respectively
λ	decay rate of liquid phase solute [t^{-1}]
$\lambda*$	decay rate of sorbed solute [t^{-1}]
$\Lambda_1,\ldots,\Lambda_6$	defined in eqns (17a)–(17d), (21) and (30), respectively
ξ	dummy integration variable
ρ	bulk density of the solid matrix (solids mass/ aquifer volume) [M L^{-3}]
τ	dummy integration variable
ϕ	Laplace transform variable with respect to spatial coordinate z
Φ	defined in eqn (A8)
ψ_m	finite Fourier cosine transform variable with respect to spatial coordinate z, defined in eqn (31)
Ψ	defined in eqn (B6)
ω	Fourier transform variable with respect to spatial coordinate y

1 INTRODUCTION

Mathematical modeling of contaminant transport in porous media has increasingly captured the attention of several environmental engineers and scientists because of the public concern, and the widespread attention paid to the disposal, movement and fate of toxic contaminants in natural subsurface systems. As the number of contaminated sites increases, so does the need for understanding the transport

and fate of contaminants in the subsurface. For well-defined, ideal aquifers, analytical solute transport models are frequently employed. Furthermore, analytical models are often used for verifying the accuracy of numerical solutions to complex solute transport models.

Multidimensional contaminant transport models have several advantages over one-dimensional models. For example, multidimensional models can account for concentration gradients and contaminant transport in directions perpendicular to the groundwater flow. As indicated by Leij and Dane,[14] measuring experimentally lateral and vertical dispersion coefficients is not a trivial task. However, multidimensional transport models can provide such parameters by direct fitting of available experimental data. In addition, multidimensional models can easily account for a variety of boundary conditions, as well as contaminant source geometries.

Although several multidimensional analytical models for solute or colloid/virus transport are available in the literature,[1,3–5,8,10,14,15,20,22,23] multidimensional analytical models that can accommodate a variety of contamination source configurations in porous media with semi-infinite or finite thickness are nonexistent.

The present study extends the collection of contaminant transport models by presenting analytical solutions to multidimensional transport through saturated, homogeneous porous media, accounting for first-order decay of the solute in the aqueous phase or sorbed onto the solid matrix with different decay rates. A variety of source configurations, including continuous as well as periodic source loadings from either point or elliptic source geometries, are considered. Generalized analytical solutions applicable to solute as well as virus transport in aquifers of semi-infinite and finite thickness are derived.

2 MODEL DEVELOPMENT

The transport of solutes in saturated, homogeneous porous media, accounting for three-dimensional hydrodynamic dispersion in a uniform flow field, nonequilibrium sorption, and first-order decay of liquid phase and sorbed solutes with different decay rates, is governed by the following partial differential equation:

$$
\frac{\partial C(t,x,y,z)}{\partial t} + \frac{\rho}{\theta}\frac{\partial C^*(t,x,y,z)}{\partial t} - D_x\frac{\partial^2 C(t,x,y,z)}{\partial x^2}
$$
$$
- D_y\frac{\partial^2 C(t,x,y,z)}{\partial y^2} - D_z\frac{\partial^2 C(t,x,y,z)}{\partial z^2}
$$
$$
+ U\frac{\partial C(t,x,y,z)}{\partial x} + \lambda C(t,x,y,z)
$$
$$
+ \lambda^*\frac{\rho}{\theta}C^*(t,x,y,z) = F(t,x,y,z), \tag{1}
$$

where C is the liquid phase solute concentration; C^* is the solute concentration sorbed onto the solid matrix; D_x, D_y and D_z are the longitudinal, lateral and vertical hydrodynamic dispersion coefficients, respectively; U is the average

interstitial velocity; t is time; x, y and z are the spatial coordinates in the longitudinal, lateral and vertical directions, respectively; ρ is the bulk density of the solid matrix; θ is the porosity of the porous medium; λ is the decay rate of liquid phase solutes; λ^* is the decay rate of sorbed solutes; and F is a general form of the source configuration. It should be noted that the effective porosity, defined as percentage of interconnected pore space, may be employed instead of porosity in a porous medium that contains a large number of dead-end pores or in a fractured porous formation.[2,7]

The accumulation of solutes onto the solid matrix is described by the following nonequilibrium expression:

$$
\frac{\rho}{\theta}\frac{\partial C^*(t,x,y,z)}{\partial t} = r_1 C(t,x,y,z) - r_2\frac{\rho}{\theta}C^*(t,x,y,z)
$$
$$
- \lambda^*\frac{\rho}{\theta}C^*(t,x,y,z), \tag{2}
$$

where r_1 and r_2 are the forward and reverse rate coefficients.

Assuming that initially there are no sorbed solutes present in the porous formation, the expression describing C^* is obtained by solving eqn (2) subject to the initial condition $C^*(0,x,y,z) = 0$ to yield

$$
C^*(t,x,y,z) = \frac{r_1\theta}{\rho}\int_0^t C(\tau,x,y,z)\exp\left[-(r_2 + \lambda^*)(t-\tau)\right]d\tau, \tag{3}
$$

where τ is a dummy integration variable. In view of eqns (2) and (3), the governing equation, eqn (1), can be written as

$$
\frac{\partial C(t,x,y,z)}{\partial t} - D_x\frac{\partial^2 C(t,x,y,z)}{\partial x^2} - D_y\frac{\partial^2 C(t,x,y,z)}{\partial y^2}
$$
$$
- D_z\frac{\partial^2 C(t,x,y,z)}{\partial z^2} + U\frac{\partial C(t,x,y,z)}{\partial x}
$$
$$
+ \mathcal{A}C(t,x,y,z) - \mathcal{B}\int_0^t C(\tau,x,y,z)e^{-\mathcal{H}(t-\tau)}\,d\tau
$$
$$
= F(t,x,y,z), \tag{4}
$$

where the following substitutions have been employed

$$
\mathcal{A} = r_1 + \lambda, \tag{5}
$$
$$
\mathcal{B} = r_1 r_2, \tag{6}
$$
$$
\mathcal{H} = r_2 + \lambda^*. \tag{7}
$$

The derived integrodifferential equation, eqn (4), is solved analytically in the subsequent sections for the cases of aquifers with semi-infinite and finite thickness.

2.1 Source configuration

The source configuration is represented by the following general function:

$$
F(t,x,y,z) = G(t)W(x,y,z), \tag{8}
$$

where $G(t)$ is the solute mass release rate per unit source

area and $W(x,y,z)$ characterizes the source physical geometry. In this work, point as well as two-dimensional source geometries are considered. Furthermore, $G(t)$ characterizes the source loading type. Although instantaneous or continuous/temporally periodic source loading types can easily be employed, the present research efforts focus only on a continuous/temporally periodic source loading.

2.1.1 Point source geometry

The point source geometry is described mathematically by the following expression:

$$W(x,y,z) = \frac{1}{\theta}\delta(x - l_{x_0})\delta(y - l_{y_0})\delta(z - l_{z_0}), \qquad (9)$$

where $l_{x_0}, l_{y_0}, l_{z_0}$ represent the x,y,z unbounded $(-\infty < l_{x_0}, l_{y_0}, l_{z_0} < \infty)$ Cartesian coordinates of the point source, respectively, and δ is the Dirac delta function. It should be noted that here G represents the solute mass release from the point source.

2.1.2 Elliptic source geometry

The elliptic source geometry is described mathematically by the following expression:

$$W(x,y,z) = \begin{cases} \dfrac{\delta(z - l_{z_0})}{\theta} & \dfrac{(x - l_{x_0})^2}{a^2} + \dfrac{(y - l_{y_0})^2}{b^2} \le 1, \\ \\ 0 & \text{otherwise}, \end{cases}$$

$$(10)$$

where $l_{x_0}, l_{y_0}, l_{z_0}$ are x,y,z Cartesian coordinates, respectively, of the center of the elliptic source geometry, and a and b represent the semi-axes of the ellipse parallel to the x- and y-axes, respectively. It should be noted that here G signifies the solute mass release rate per unit source area.

2.2 Aquifer with semi-infinite thickness

The appropriate initial and boundary conditions for the case of an aquifer with infinite longitudinal and lateral directions and semi-infinite vertical direction (thickness), as illustrated schematically in Fig. 1(a), are as follows:

$$C(0,x,y,z) = 0, \qquad (11)$$

$$C(t, \pm\infty, y, z) = 0, \qquad (12)$$

$$C(t, x, \pm\infty, z) = 0, \qquad (13)$$

$$\frac{\partial C(t,x,y,0)}{\partial z} = 0, \qquad (14)$$

$$\frac{\partial C(t,x,y,\infty)}{\partial z} = 0, \qquad (15)$$

where condition (11) corresponds to the situation in which solutes are initially absent from the three-dimensional porous formation, eqns (12) and (13) indicate that the aquifer is infinite horizontally and laterally, boundary condition (14) represents a zero dispersive flux boundary and eqn

(15) preserves concentration continuity for a semi-infinite vertical aquifer thickness. The vertical level $z = 0$ defines the location of the water table or a confining layer. Eqn (4), subject to conditions (11)–(15), is solved analytically. It should be noted that z increases in the downward direction.

The analytical solution to the governing partial differential equation, eqn (4), can be derived by a variety of methods, including the conventional method of separation of variables, as well as integral transform methods. Furthermore, a solution technique developed by Walker[24] involving a Green function (fundamental solution) can also be utilized. However, in the present study, integral transform techniques were employed because the multidimensional models developed are an extension of our previous analytical work on virus transport models,[19,20] where Laplace transform techniques were employed. Similar mathematical techniques were employed for the analytical solutions of multidimensional solute transport by Toride *et al.*[21] and Shan and Javandel.[18]

Taking Laplace transforms with respect to time variable t and space variable z, and Fourier transforms with respect to space variables x and y of eqn (4), and subsequently employing the transformed initial and boundary conditions, followed by inverse transformations, yields the desired analytical solution for an aquifer with semi-infinite thickness
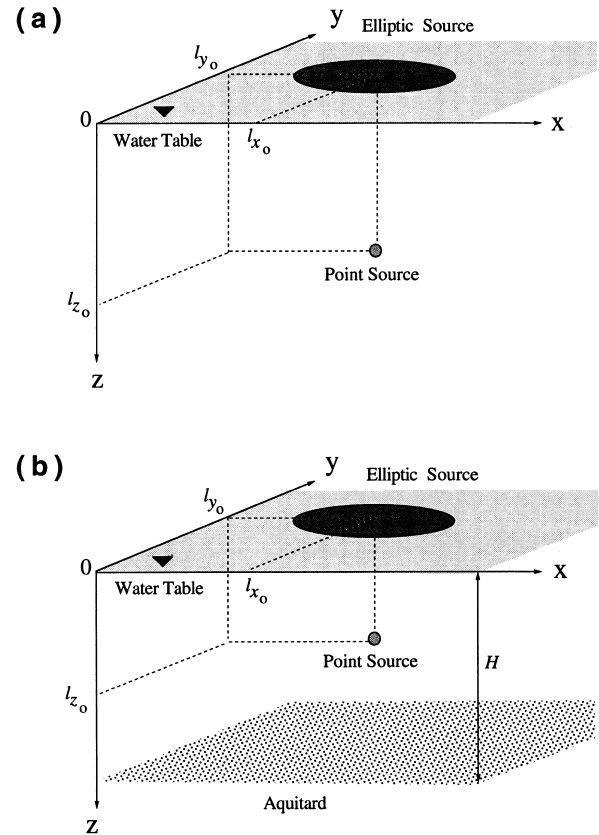

Fig. 1. Schematic illustration of point and elliptic sources of contamination with coordinates $l_{x_0}, l_{y_0}, l_{z_0}$ in an aquifer with semi-infinite (a) and finite (b) thickness. Note that the positive direction for the vertical coordinate is inverted.

(see Appendix A):

$$C(t,x,y,z) = \left(\frac{1}{64\pi^3 D_x D_y D_z}\right)^{1/2} \int_0^t \int_{-\infty}^{\infty} \int_{-\infty}^{\infty} \int_0^{\infty}$$

$$\times F(t-\tau,q,v,p)\Lambda_1(\tau)$$

$$\times \left\{\int_0^{\tau} \frac{\Lambda_2(\tau)}{\zeta^{3/2}}\Lambda_3(\zeta,x-q,y-v)\left[\Lambda_4(\zeta,z+p)\right.\right.$$

$$\left.+\Lambda_4(\zeta,z-p)\right]d\zeta + \frac{\Lambda_3(\tau,x-q,y-v)}{\tau^{3/2}}$$

$$\times \left[\Lambda_4(\tau,z+p)+\Lambda_4(\tau,z-p)\right]\Bigg\} dp\,dv\,dq\,d\tau,$$

$$(16)$$

where p, q, v and ζ are dummy integration variables; the following definitions were employed:

$$\Lambda_1(t) = \exp[-\mathcal{H}t], \tag{17a}$$

$$\Lambda_2(t) = \left(\frac{\mathcal{B}\zeta}{t-\zeta}\right)^{1/2} I_1\left[2\left(\mathcal{B}\zeta(t-\zeta)\right)^{1/2}\right], \tag{17b}$$

$$\Lambda_3(t,x,y) = \exp\left[\frac{Ux}{2D_x} - \frac{1}{4t}\left(\frac{x^2}{D_x}+\frac{y^2}{D_y}\right)\right.$$

$$\left.-t\left(\mathcal{A}-\mathcal{H}+\frac{U^2}{4D_x}\right)\right], \tag{17c}$$

$$\Lambda_4(t,z) = \exp\left[\frac{-z^2}{4D_z t}\right], \tag{17d}$$

and I_1 is the modified Bessel function of the first kind of first order.

2.2.1 Point source geometry

Substituting eqns (8) and (9) into eqn (16) yields the analytical solution for the case of point source geometry:

$$C(t,x,y,z) = \left(\frac{1}{64\pi^3 D_x D_y D_z}\right)^{1/2} \int_0^t \frac{G(t-\tau)}{\theta}\Lambda_1(\tau)$$

$$\times \left\{\int_0^{\tau} \frac{\Lambda_2(\tau)}{\zeta^{3/2}}\Lambda_3(\zeta,x-l_{x_0},y-l_{y_0})\right.$$

$$\times \left[\Lambda_4(\zeta,z+l_{z_0})+\Lambda_4(\zeta,z-l_{z_0})\right]d\zeta$$

$$+\frac{\Lambda_3(\tau,x-l_{x_0},y-l_{y_0})}{\tau^{3/2}}$$

$$\times \left[\Lambda_4(\tau,z+l_{z_0})+\Lambda_4(\tau,z-l_{z_0})\right]\Bigg\} d\tau, \tag{18}$$

where Λ_1–Λ_4 are defined in eqns (17a)–(17d), respectively, and the following property of the Dirac delta function was employed:

$$\int_{\alpha}^{\beta} f_0(t)\delta(t-t_0)\,dt = f_0(t_0), \qquad \alpha \leq t_0 \leq \beta, \tag{19}$$

where α and β are arbitrary constants, and f_0 is an arbitrary function.

2.2.2 Elliptic source geometry

Substituting eqns (8) and (10) into eqn (16) leads to the analytical solution for the case of elliptic source geometry:

$$C(t,x,y,z) = \left(\frac{1}{64\pi^2 D_x D_z}\right)^{1/2} \int_0^t \int_{a_1}^{a_2} \frac{G(t-\tau)}{\theta}\Lambda_1(\tau)$$

$$\times \left\{\int_0^{\tau} \frac{\Lambda_2(\tau)}{\zeta}\Lambda_3(\zeta,x-q,0)\left[\Lambda_4(\zeta,z+l_{z_0})\right.\right.$$

$$\left.+\Lambda_4(\zeta,z-l_{z_0})\right]\Lambda_5(\zeta)\,d\zeta + \frac{\Lambda_3(\tau,x-q,0)}{\tau}$$

$$\times \left[\Lambda_4(\tau,z+l_{z_0})+\Lambda_4(\tau,z-l_{z_0})\right]\Lambda_5(\tau)\Bigg\} dq\,d\tau,$$

$$(20)$$

where Λ_1–Λ_4 are defined in eqns (17a)–(17d), respectively,

$$\Lambda_5(t) = \text{erf}\left[\kappa_1(t,q,y)\right] - \text{erf}\left[\kappa_2(t,q,y)\right], \tag{21}$$

$$a_1 = l_{x_0} - a, \tag{22}$$

$$a_2 = l_{x_0} + a, \tag{23}$$

$$\kappa_1(t,q,y) = \left\{y-l_{y_0}+\left[b^2-\frac{b^2(q-l_{x_0})^2}{a^2}\right]^{1/2}\right\}\left(\frac{1}{4D_y t}\right)^{1/2},$$

$$(24)$$

$$\kappa_2(t,q,y) = \left\{y-l_{y_0}-\left[b^2-\frac{b^2(q-l_{x_0})^2}{a^2}\right]^{1/2}\right\}\left(\frac{1}{4D_y t}\right)^{1/2},$$

$$(25)$$

erf[·] is the error function, and the following transformation and integral relationships were employed:

$$\kappa = \frac{y-v}{(4tD_y)^{1/2}} \tag{26a}$$

$$d\kappa = \frac{-dv}{(4tD_y)^{1/2}}, \tag{26b}$$

$$\int_{\kappa_1}^{\kappa_2} \exp[-\kappa^2]\,d\kappa = \frac{-\pi^{1/2}}{2}\left\{\text{erf}\left[\kappa_1\right]-\text{erf}\left[\kappa_2\right]\right\}. \tag{27}$$

As noted by Chrysikopoulos,[4] solving for an elliptic source geometry is advantageous because the appropriate solution for a circular source can easily be obtained by setting $a = b = r$ in eqns (22)–(25), where r is the radius of the circular source.

2.3 Aquifer with finite thickness

The desired analytical solution for the case of an aquifer with finite thickness, as illustrated schematically in Fig. 1(b), is obtained by solving eqn (4) subject to conditions (11)–(14) and the following finite vertical, lower boundary condition:

$$\frac{\partial C(t,x,y,H)}{\partial z} = 0, \tag{28}$$

where H is the aquifer thickness. The boundary condition

(28) implies that the aquifer is confined by an impermeable layer at depth $z = H$. Taking the Laplace transform with respect to the time variable t, Fourier transforms with respect to space variables x and y, and the finite Fourier cosine transform with respect to the space variable z of eqn (4), and subsequently employing the transformed initial and boundary conditions, followed by inverse transformations yields (see Appendix B):

$$C(t,x,y,z) = \left(\frac{1}{16\pi^2 D_x D_y}\right)^{1/2} \int_0^t \int_{-\infty}^{\infty} \int_{-\infty}^{\infty} \Lambda_1(\tau)$$

$$\times \left\{ \int_0^\tau \frac{\Lambda_2(\tau)}{\zeta} \Lambda_3(\zeta, x-q, y-v) \right.$$

$$\times \Lambda_6\big(\zeta, \ddot{F}(t-\tau, q, v, 0), \ddot{F}(t-\tau, q, v, \psi_m)\big) \, d\zeta$$

$$+ \frac{\Lambda_3(\tau, x-q, y-v)}{\tau} \Lambda_6\big(\tau, \ddot{F}(t-\tau, q, v, 0),$$

$$\times \left. \ddot{F}(t-\tau, q, v, \psi_m)\big) \right\} \, dv \, dq \, d\tau, \qquad (29)$$

where Λ_1–Λ_3 are defined in eqns (17a)–(17c), respectively,

$$\Lambda_6(t, f_1, f_2) = \frac{f_1}{H} + \frac{2}{H} \sum_{m=1}^{\infty} f_2 \exp\big[-\psi_m^2 D_z t\big] \cos(\psi_m z), \tag{30}$$

$$\psi_m = \frac{m\pi}{H}, \tag{31}$$

m is the integer summation index, $\ddot{F}(t, x, y, \psi_m)$ represents the finite Fourier cosine transform of $F(t,x,y,z)$ with respect to space variable z with corresponding finite Fourier cosine transform variable ψ_m, and f_1 and f_2 are arbitrary functions.

2.3.1 Point source geometry

The desired analytical solution for the case of point source geometry is obtained by substituting the corresponding expression for $\ddot{F}(t, x, y, \psi_m)$ into eqn (29). Substituting eqn (9) into eqn (8) and subsequently taking the finite Fourier cosine transform (defined in eqn (B3)) with respect to space variable z of the resulting expression yields

$$\ddot{F}(t, x, y, \psi_m) = \int_0^H \frac{G(t)}{\theta} \delta(x-l_{x_0}) \delta(y-l_{y_0}) \delta(z-l_{z_0})$$

$$\times \cos(\psi_m z) \, dz = \frac{G(t)}{\theta} \delta(x-l_{x_0}) \delta(y-l_{y_0})$$

$$\times \cos(\psi_m l_{z_0}), \tag{32}$$

where the latter formulation in eqn (32) is a consequence of employing eqn (19). In view of eqns (19) and (32), the general solution, eqn (29), reduces to the following form:

$$C(t,x,y,z) = \left(\frac{1}{16\pi^2 D_x D_y}\right)^{1/2} \int_0^t \frac{G(t-\tau)}{\theta} \Lambda_1(\tau)$$

$$\times \left\{ \int_0^\tau \frac{\Lambda_2(\tau)}{\zeta} \Lambda_3(\zeta, x-l_{x_0}, y-l_{y_0}) \right.$$

$$\times \Lambda_6\big(\zeta, 1, \cos(\psi_m l_{z_0})\big) \, d\zeta$$

$$+ \frac{\Lambda_3(\tau, x-l_{x_0}, y-l_{y_0})}{\tau}$$

$$\times \left. \Lambda_6\big(\tau, 1, \cos(\psi_m l_{z_0})\big) \right\} \, d\tau, \tag{33}$$

where Λ_1–Λ_3 and Λ_6 are defined in eqns (17a)–(17c) and (30), respectively.

2.3.2 Elliptic source geometry

In view of eqn (10), the finite Fourier cosine transform of eqn (8) with respect to z is given by

$$\ddot{F}(t,x,y,\psi_m) = \begin{cases} \dfrac{G(t)}{\theta} \cos(\psi_m l_{z_0}) & \dfrac{(x-l_{x_0})^2}{a^2} + \dfrac{(y-l_{y_0})^2}{b^2} \leq 1, \\ 0 & \text{otherwise.} \end{cases} \tag{34}$$

Substituting eqn (34) into eqn (29), the desired analytical solution for the case of elliptic source geometry is as follows:

$$C(t,x,y,z) = \left(\frac{1}{16\pi D_x}\right)^{1/2} \int_0^t \int_{a_1}^{a_2} \frac{G(t-\tau)}{\theta} \Lambda_1(\tau)$$

$$\times \left\{ \int_0^\tau \frac{\Lambda_2(\tau)}{\zeta^{1/2}} \Lambda_3(\zeta, x-q, 0) \Lambda_5(\zeta) \right.$$

$$\times \Lambda_6\big(\zeta, 1, \cos(\psi_m l_{z_0})\big) \, d\zeta + \frac{\Lambda_3(\tau, x-q, 0)}{\tau^{1/2}}$$

$$\times \left. \Lambda_5(\tau) \Lambda_6\big(\tau, 1, \cos(\psi_m l_{z_0})\big) \right\} \, dq \, d\tau, \tag{35}$$

where a_1 and a_2 are defined in eqns (22) and (23), respectively, and Λ_1–Λ_3, Λ_5 and Λ_6 are defined in eqns (17a)–(17c), (21) and (30), respectively.

3 MODEL SIMULATIONS AND DISCUSSION

Model simulations are performed for two different source configurations, and aquifers with either semi-infinite or finite thickness. The integrals present in the analytical solutions (18), (20), (33) and (35) are evaluated numerically by the integration routines Q1DA and QDAG, which utilize globally adaptive quadrature algorithms.[11,12] The infinite series part of the solution for the case of an aquifer with finite thickness (eqn (30)) is evaluated by considering up to 1000 terms ($m = 1000$). The number of terms, m, is selected so that additional terms do not alter the summation more than 0.001%.

The groundwater table and the bottom of the finite thickness aquifer are assumed to be located at $z = 0$ cm and $z = H = 100$ cm, respectively. Although all analytical solutions derived here are general enough to account for temporally

Table 1. Model parameters for simulations

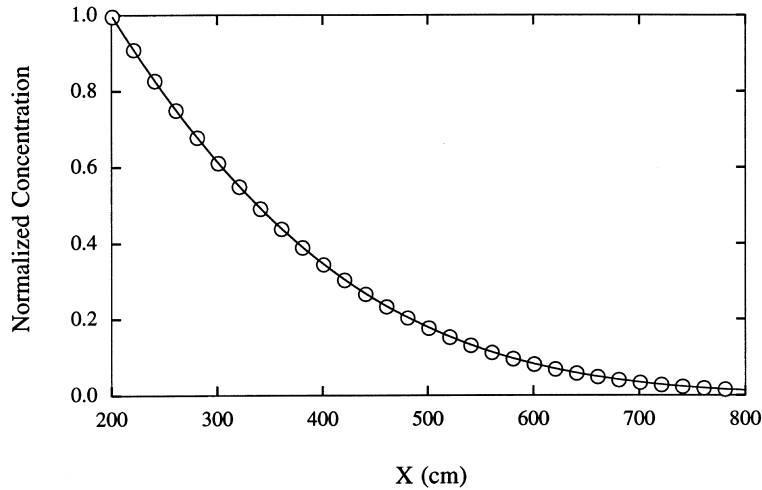| Parameter	Value	Reference
D_x	1331.25 cm^2 h^{-1}	Batu[1]
$D_y = D_z$	268.75 cm^2 h^{-1}	Batu[1]
U	0.625 cm h^{-1}	Batu[1]
$\lambda = \lambda^*$	0 days	—
ρ	1.5 g cm^{-3}	Yates and Ouyang[25]
θ	0.25	Park et al.[16]

Fig. 2. Comparison between the analytical solution derived in this work for a point source geometry with constant mass release rate (solid curve) and the corresponding solution of the one-dimensional model presented by Sim and Chrysikopoulos[19] (circles). Here, $D_y = D_z \simeq$ $0 \, \text{cm}^2 \, \text{h}^{-1}$, $l_{x_0} = 200$ cm, $l_{y_0} = 0$ cm, $l_{z_0} = 50$ cm, $r_1 = 0.03 \, \text{h}^{-1}$, $r_2 = 0.017 \, \text{h}^{-1}$, $t = 1$ day, $y = 0.1$cm and $z = 50$ cm.
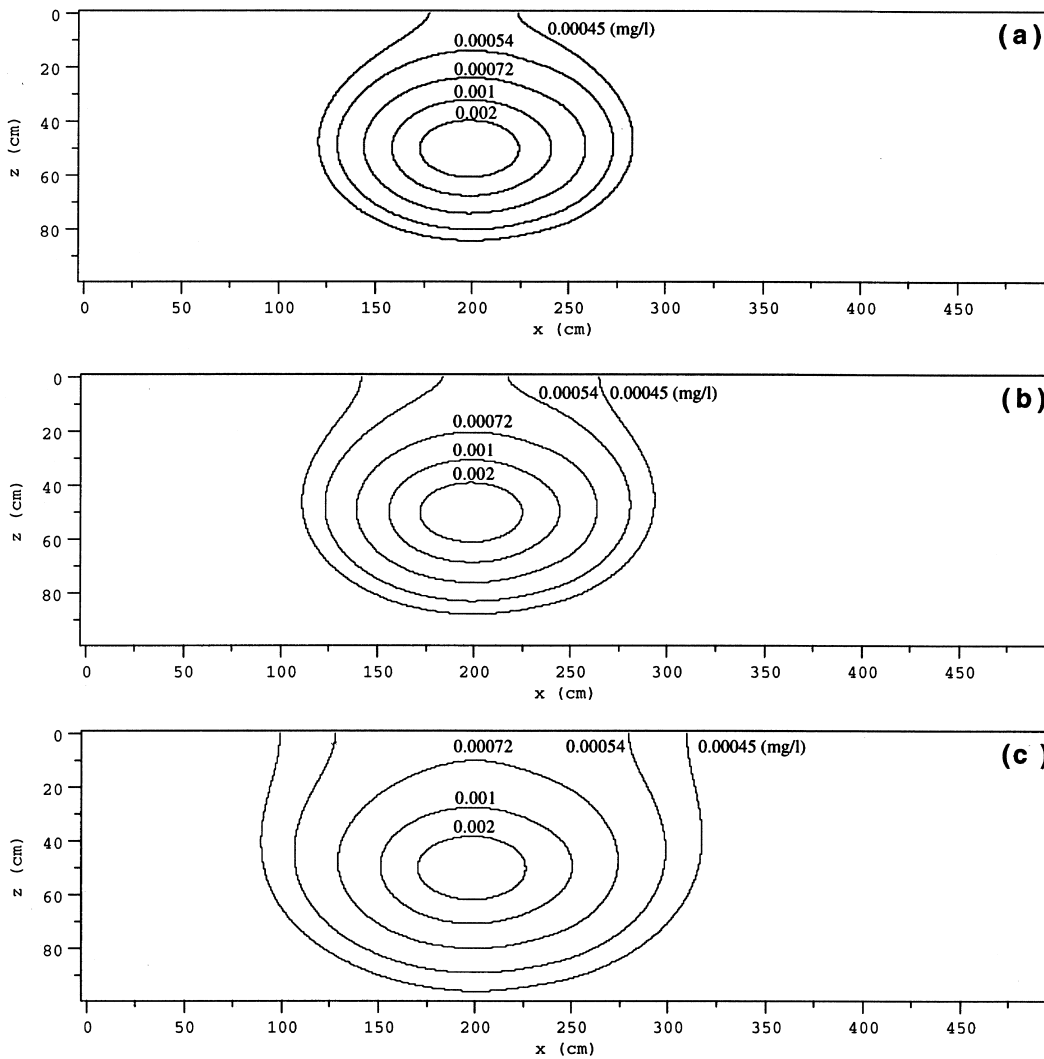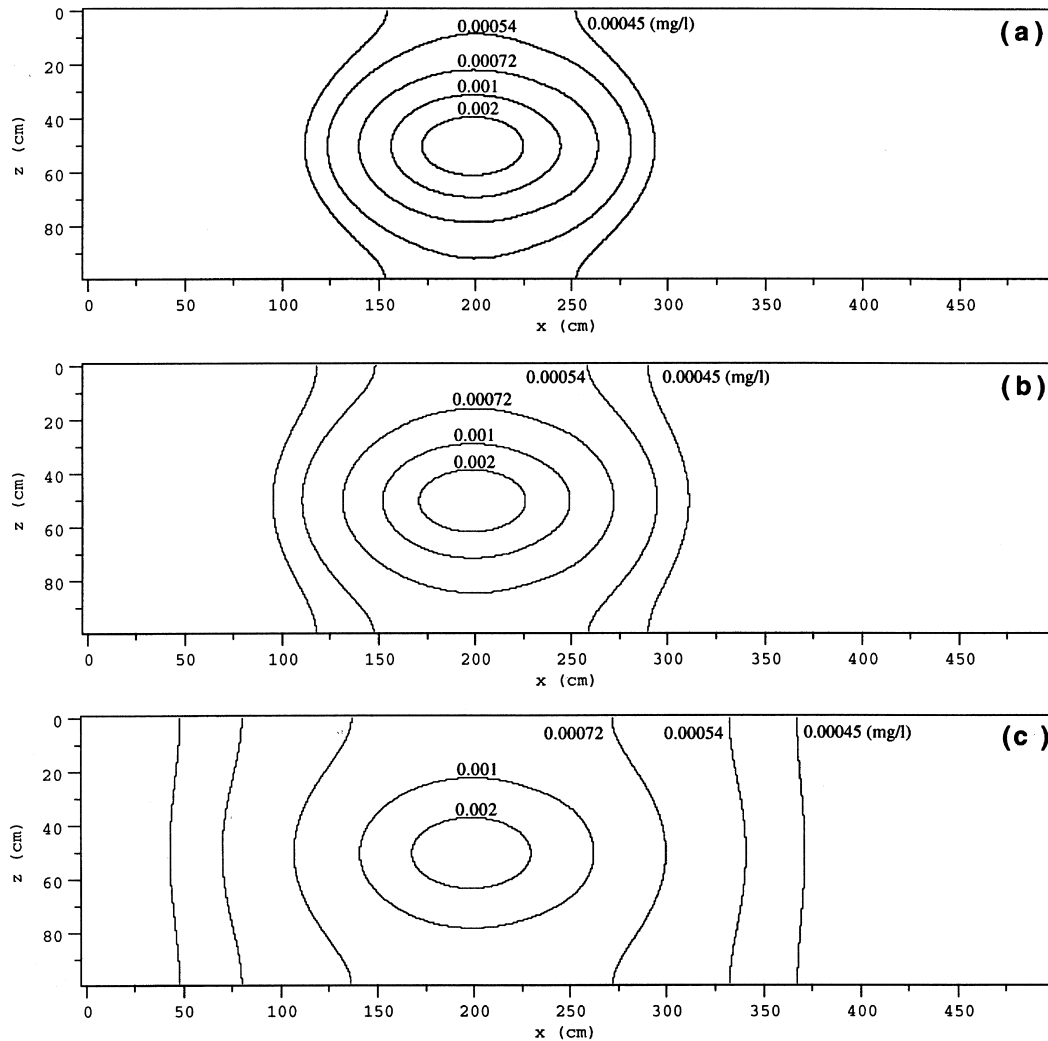

Fig. 3. Concentration contours in the x–z plane obtained for a point source within an aquifer of semi-infinite thickness at $t = 50$ days (a), $t = 100$ days (b) and $t = 300$ days (c). Here, $l_{x_0} = 200$ cm, $l_{y_0} = 0$ cm, $l_{z_0} = 50$ cm, $r_1 = 0.1 \, \text{h}^{-1}$, $r_2 = 0.0008 \, \text{h}^{-1}$ and $y = 0$ cm.

Fig. 4. Concentration contours in the x–z plane obtained for a point source within an aquifer of finite thickness at $t = 50$ days (a), $t = 100$ days (b) and $t = 300$ days (c). Here, $l_{x_0} = 200$ cm, $l_{y_0} = 0$ cm, $l_{z_0} = 50$ cm, $r_1 = 0.03$ h^{-1}, $r_2 = 0.017$ h^{-1} and $y = 0$ cm.

periodic source loading, for simplicity, the model simulations presented are based on a constant solute mass release rate and the value of G is set to unity. Unless otherwise specified, the fixed parameter values used in the simulations are those listed in Table 1.

For the case where $D_y = D_z \simeq 0$ cm^2 h^{-1}, the analytical solution derived in this work for a point source geometry with constant solute mass release rate is equivalent to the one-dimensional analytical solution for virus transport with constant concentration boundary conditions presented by Sim and Chrysikopoulos[19] (eqn (31)). For this special case, model simulations are compared in Fig. 2 against the one-dimensional model derived by Sim and Chrysikopoulos.[19] It should be noted, however, that in Fig. 2 the concentrations simulated by the one-dimensional transport model (circles) are normalized with the source concentration (C_0), whereas concentrations generated by solutions derived in this work (solid curves) are normalized with the steady-state concentration (C_∞) evaluated at $t = 400$ days, as suggested by Hunt.[10] Fig. 2 clearly indicates

that the model simulations compared are virtually identical.

Fig. 3 illustrates two-dimensional snapshots of solute concentration at three successive times simulated for an aquifer with semi-infinite thickness (eqn (18)). A point source is assumed to be located inside the aquifer at $l_{x_0} = 200$ cm, $l_{y_0} = 0$ cm and $l_{z_0} = 50$ cm. It is observed that as the solute plume spreads with increasing time, solute spreading is restricted at the groundwater table ($z = 0$ cm), with a consequent zero gradient of solute concentration distribution, whereas a continuous solute spreading occurs anywhere else below the water table because the aquifer extends to infinity without a boundary (eqn (15)). Consequently, the observed solute plume is asymmetric with respect to the flow direction along the plume centerline. In contrast, Fig. 4 illustrates symmetric solute plumes at three successive times, for an aquifer with finite thickness and point source geometry (eqn (33)). This is due to the presence of a fixed impermeable lower boundary (eqn (28), $z = H = 100$ cm) in addition to the upper groundwater
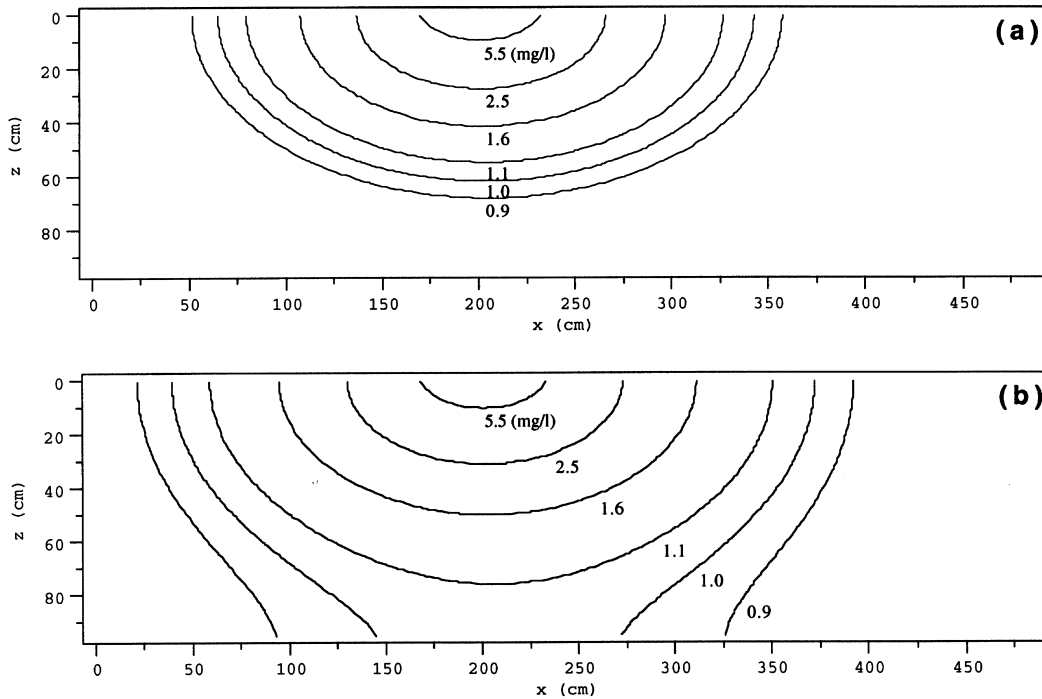
Fig. 5. Concentration contours in the x–z plane obtained for an elliptic source geometry, and an aquifer with semi-infinite (a) and finite (b) thickness. Here, $a = b = 25$ cm, $l_{x_0} = 200$ cm, $l_{y_0} = l_{z_0} = 0$ cm, $r_1 = 0.1$ h^{-1}, $r_2 = 0.0008$ h^{-1}, $t = 300$ days and $y = 0$ cm.

table boundary ($z = 0$ cm). Comparing Figs 3 and 4, it is clear that the vertical migration of solutes is hindered by the two fixed boundaries. Furthermore, the presence of these boundaries contributes to the enhancement of solute transport downstream from the source in the direction of groundwater flow.

The effect of the lower impermeable boundary condition is also demonstrated for the case of an elliptic source geometry. Two-dimensional snapshots of solute concentrations at $t = 300$ days are predicted for the case of an elliptic source geometry for an aquifer with semi-infinite thickness (eqn (20), Fig. 5(a)), as well as for an aquifer with finite thickness (eqn (35), Fig. 5(b)). Similarly to the case of point source geometry, the presence of a shallow impermeable aquitard significantly constricts the vertical spreading of solutes, which consequently leads to an enhanced solute migration in the direction of groundwater flow.

The analytical solutions derived in this work can be readily employed to simulate transport of a variety of contaminants, including biocolloids such as viruses and bacteria. The applicability of these models to field investigations is limited to subsurface formations, where it may not be possible to account for physicochemically heterogeneous porous media. However, it should be noted that multidimensional contaminant transport models are more advantageous than one-dimensional models where a homogeneous porous medium assumption is valid, because they can account for concentration gradients and contaminant transport in directions perpendicular to the groundwater flow. Furthermore, multidimensional models can easily

account for a variety of boundary conditions, as well as contaminant source geometries.

4 SUMMARY

Three-dimensional analytical solutions for solute transport in saturated, homogeneous porous media were developed, accounting for three-dimensional hydrodynamic dispersion in a uniform flow field, first-order decay of aqueous phase and sorbed solutes with different decay rates, and nonequilibrium solute sorption onto the solid matrix of the porous formation. The governing transport equations were solved analytically by employing Laplace, Fourier and finite Fourier cosine transform techniques. Aquifers with either semi-infinite or finite thickness are considered. The derived analytical solutions are general enough to accommodate a variety of source loadings and source geometries. However, the simulations presented in this study are based on a continuous source loading from either point source or elliptic source geometry. It was shown that solute transport in subsurface porous media is significantly influenced by the aquifer boundary conditions. For an aquifer confined by a shallow impermeable aquitard, solute migration in the vertical direction is restricted, whereas solute transport in the direction of groundwater flow is enhanced, compared with the case of a relatively thick aquifer. The analytical solutions developed here are particularly useful for preliminary estimation of solute migration, characterization of

contamination sources, examination of possible aquifer boundary conditions, validation of numerical solutions and determination of solute transport parameters from laboratory or well-defined field experiments.

REFERENCES

1. Batu, V. A generalized two-dimensional analytical solute transport model in bounded media for flux-type finite multiple sources. *Water Resour. Res.*, 1993, **29**(8), 1125–1132.
2. Bear, J., *Dynamics of Fluids in Porous Media*. Dover, 1972.
3. Bellin, A., Rinaldo, A., Bosma, W. J. P., van der Zee, S. E. A. T. M. and Rubin, Y. Linear equilibrium adsorbing solute transport in physically and chemically heterogeneous porous formations. 1. Analytical solutions. *Water Resour. Res.*, 1993, **29**(12), 4019–4030.
4. Chrysikopoulos, C. V. Three-dimensional analytical models of contaminant transport from nonaqueous phase liquid pool dissolution in saturated subsurface formations. *Water Resour. Res.*, 1995, **31**(4), 1137–1145.
5. Chrysikopoulos, C. V., Voudrias, E. A. and Fyrillas, M. M. Modeling of contaminant transport resulting from dissolution of nonaqueous phase liquid pools in saturated porous media. *Trans. Porous Media*, 1994, **16**(2), 125–145.
6. Churchill, R. V., *Operational Mathematics*. McGraw-Hill, New York, 1958.
7. Domenico, P. A. & Schwartz, F. W., *Physical and Chemical Hydrogeology*. John Wiley, New York, 1990.
8. Goltz, M. N. and Roberts, P. V. Three-dimensional solutions for solute transport in an infinite medium with mobile and immobile zones. *Water Resour. Res.*, 1986, **22**(7), 1139–1148.
9. Gradshteyn, I. S. & Ryzhik, I. M., *Table of Integral, Series, and Products*. Academic Press, New York, 1980.
10. Hunt, B. Dispersive sources in uniform groundwater flow. *J. Hydraul. Div., Am. Soc. Civ. Engng*, 1978, **104**(HY1), 75–85.
11. IMSL, *IMSL MATH/LIBRARY User's Manual*, version 2.0. IMSL, Houston, 1991.
12. Kahaner, D., Moler, C. & Nash, S., *Numerical Methods and Software*. Prentice Hall, Englewood Cliffs, NJ, 1989.
13. Kreyszig, E., *Advanced Engineering Mathematics*, 7th ed. John Wiley, New York, 1993.
14. Leij, F. J. and Dane, J. H. Analytical solutions of the one-dimensional advection equation and two- or three-dimensional dispersion equation. *Water Resour. Res.*, 1990, **26**(7), 1475–1482.
15. Leij, F. J., Skaggs, T. H. and van Genuchten, M. Th. Analytical solutions for solute transport in three-dimensional semi-infinite porous media. *Water Resour. Res.*, 1991, **27**(10), 2719–2733.
16. Park, N., Blanford, T. N. & Huyakorn, P. S., *VIRALT: A Modular Semi-analytical and Numerical Model for Simulating Viral Transport in Ground Water*. International Ground Water Modeling Center, Colorado School of Mines, Golden, CO, 1992.
17. Roberts, G. E. & Kaufman, H., *Table of Laplace Transforms*. W. B. Saunders, Philadelphia, PA, 1966.
18. Shan, C. and Javandel, I. Analytical solutions for solute transport in a vertical aquifer section. *J. Contam. Hydrol.*, 1997, **27**(1)2, 63–82.
19. Sim, Y. & Chrysikopoulos, C. V., Analytical models for one-dimensional virus transport in saturated porous media. *Water Resour. Res.*, **31**(5) (1995) 1429–1437. [Correction, *Water Resour. Res.*, **32**(5), (1996) 1473].
20. Sim, Y. and Chrysikopoulos, C. V. Three-dimensional analytical models for virus transport in saturated porous media. *Transport in Porous Media*, 1998, **30**(1), 87–112.
21. Toride, N., Leij, F. J. and Van Genuchten, M. T. A comprehensive set of analytical solutions for nonequilibrium solute transport with 1st-order decay and zero-order production. *Water Resour. Res.*, 1993, **29**(7), 2167–2182.
22. van Dujin, C. J. and van der Zee, S. E. A. T. M. Solute transport parallel to an interface separating two different porous materials. *Water Resour. Res.*, 1986, **22**(13), 1779–1789.
23. van Kooten, J. J. A. A method to solve the advection–dispersion equation with a kinetic adsorption isotherm. *Adv. Water Resour.*, 1996, **19**(4), 193–206.
24. Walker, G. R. Solution to a class of coupled linear partial differential equations. *IMA J. Appl. Math.*, 1987, **38**, 35–48.
25. Yates, M. V. and Ouyang, Y. VIRTUS, a model of virus transport in unsaturated soils. *Appl. Environ. Microb.*, 1992, **58**(5), 1609–1616

APPENDIX A DERIVATION OF THE ANALYTICAL SOLUTION FOR AN AQUIFER WITH SEMI-INFINITE THICKNESS

The analytical solution for the case of semi-infinite thickness is obtained by solving eqn (4) subject to conditions (11)–(15). Taking Laplace transforms with respect to time variable t and space variable z, and Fourier transforms with respect to space variables x and y of eqn (4) and subsequently employing eqn (11) and transformed boundary condition (14) yields

$$\tilde{\bar{\hat{\hat{C}}}}(s,\gamma,\omega,\phi) = \frac{\phi\bar{\hat{\hat{C}}}(s,\gamma,\omega,0)}{(\phi+\mathcal{E})(\phi-\mathcal{E})} - \frac{\tilde{\bar{\hat{\hat{F}}}}(s,\gamma,\omega,\phi)}{D_z(\phi+\mathcal{E})(\phi-\mathcal{E})},$$

(A1)

where

$$\mathcal{E} = \frac{1}{D_z^{1/2}}\left(s + \gamma^2 D_x + i\gamma U + \omega^2 D_y + \mathcal{A} - \frac{\mathcal{B}}{s+\mathcal{H}}\right)^{1/2},$$

(A2)

and the following properties were employed for the Laplace and Fourier transformations:[13,17]

$$\tilde{C}(s,x,y,z) = \int_0^\infty C(t,x,y,z)e^{-st}\,dt,$$

(A3)

$$\hat{\tilde{C}}(s,\gamma,y,z) = \frac{1}{(2\pi)^{1/2}}\int_{-\infty}^\infty \tilde{C}(s,x,y,z)e^{-i\gamma x}\,dx,$$

(A4)

$$\bar{\hat{\bar{C}}}(s,\gamma,\omega,z) = \frac{1}{(2\pi)^{1/2}} \int_{-\infty}^{\infty} \hat{\bar{C}}(s,\gamma,y,z) e^{-i\omega y}\, dy, \qquad (A5)$$

$$\dot{\bar{\hat{\bar{C}}}}(s,\gamma,\omega,\phi) = \int_{0}^{\infty} \bar{\hat{\bar{C}}}(s,\gamma,\omega,z) e^{-\phi z}\, dz, \qquad (A6)$$

where the tilde and overdot signify Laplace transform with respect to time and space variables t and z, respectively, and s and ϕ are the corresponding Laplace domain variables; the hat and overbar signify Fourier transforms with respect to space variables x and y with corresponding Fourier domain variables γ and ω, respectively; and $i = (-1)^{1/2}$.

Taking the Laplace inverse transformation of eqn (A1) with respect to ϕ, applying boundary condition (15) and subsequently evaluating $\bar{\hat{\bar{C}}}(s,\gamma,\omega,0)$ at the limit $z \to \infty$, yields

$$\bar{\hat{\bar{C}}}(s,\gamma,\omega,z) = \frac{1}{2D_z}\Bigg\{ \int_{0}^{\infty} \bar{\hat{\bar{F}}}(s,\gamma,\omega,p)\big[\Phi(s,\gamma,\omega,z+p)$$
$$+\,\Phi(s,\gamma,\omega,p-z)\big]\,dp + \int_{0}^{z}\bar{\hat{\bar{F}}}(s,\gamma,\omega,p)$$
$$\times \big[\Phi(s,\gamma,\omega,z-p) - \Phi(s,\gamma,\omega,p-z)\big]\,dp\Bigg\},$$
$$(A7)$$

where

$$\Phi(s,\gamma,\omega,z) = \frac{e^{-\mathcal{E}z}}{\mathcal{E}}, \qquad (A8)$$

and the following Laplace inversion identities were utilized:[17]

$$\mathcal{L}^{-1}\{\tilde{f}_1(p)\tilde{f}_2(p)\} = \int_{0}^{z} f_1(z-p)f_2(p)\,dp, \qquad (A9)$$

$$\mathcal{L}^{-1}\left\{\frac{\phi}{(\phi+\alpha)(\phi+\beta)}\right\} = \frac{\alpha e^{-\alpha z}}{\alpha-\beta} + \frac{\beta e^{-\beta z}}{\beta-\alpha}, \qquad (A10)$$

$$\mathcal{L}^{-1}\left\{\frac{1}{(\phi+\alpha)(\phi+\beta)}\right\} = \frac{e^{-\alpha z} - e^{-\beta z}}{\beta-\alpha}, \qquad (A11)$$

where $\mathcal{L}^{-1}$ is the Laplace inverse operator, and α and β are arbitrary constants.

Furthermore, for mathematical convenience, let

$$\Phi = \frac{\mathcal{H}\Phi}{s+\mathcal{H}} + \frac{s\Phi}{s+\mathcal{H}}. \qquad (A12)$$

The inverse Laplace transformation of eqn (A12) with respect to s can be found by employing the following relationship:[19]

$$\mathcal{L}^{-1}\left\{\frac{1}{s+\mathcal{H}}\tilde{f}_0\left(s+\mathcal{H}-\frac{\alpha}{s+\mathcal{H}}\right)\right\}$$
$$= e^{-\mathcal{H}t}\int_{0}^{t} I_0\big[2(\alpha\zeta(t-\zeta))^{1/2}\big]f_0(\zeta)\,d\zeta, \qquad (A13)$$

where $\tilde{f}_0(s)$ is the Laplace transform of the arbitrary function $f_0(t)$ and α is an arbitrary constant. Following the procedures provided in Sim and Chrysikopoulos,[19] the inverse

Laplace transform of eqn (A12) is obtained as

$$\mathcal{L}^{-1}\left\{\frac{\mathcal{H}\Phi(s,\gamma,\omega,z)}{s+\mathcal{H}} + \frac{s\Phi}{s+\mathcal{H}}\right\}$$
$$= \mathcal{H}\bar{\hat{\bar{P}}}(t,\gamma,\omega,z) + \frac{\partial \bar{\hat{\bar{P}}}(t,\gamma,\omega,z)}{\partial t}, \qquad (A14)$$

where

$$\bar{\hat{\bar{P}}}(t,\gamma,\omega,z) = e^{-\mathcal{H}t}\int_{0}^{t} I_0\big[2(\mathcal{B}\zeta(t-\zeta))^{1/2}\big]\left(\frac{D_z}{\pi\zeta}\right)^{1/2}$$
$$\times \exp\left[-\frac{z^2}{4D_z\zeta} - (\omega^2 D_y + \mathcal{A} - \mathcal{H})\zeta\right]Q(\gamma,\zeta)\,d\zeta, \qquad (A15)$$

$$\frac{\partial \bar{\hat{\bar{P}}}(t,\gamma,\omega,z)}{\partial t} = e^{-\mathcal{H}t}\int_{0}^{t}\Bigg\{\left(\frac{\mathcal{B}\zeta}{t-\zeta}\right)^{1/2} I_1\big[2(\mathcal{B}\zeta(t-\zeta))^{1/2}\big]$$
$$-\mathcal{H}I_0\big[2(\mathcal{B}\zeta(t-\zeta))^{1/2}\big]\Bigg\}\times\left(\frac{D_z}{\pi\zeta}\right)^{1/2}$$
$$\times \exp\left[-\frac{z^2}{4D_z\zeta} - (\omega^2 D_y + \mathcal{A} - \mathcal{H})\zeta\right]$$
$$\times Q(\gamma,\zeta)\,d\zeta + e^{-\mathcal{H}t}\left(\frac{D_z}{\pi t}\right)^{1/2}$$
$$\times \exp\left[-\frac{z^2}{4D_z t} - (\omega^2 D_y + \mathcal{A} - \mathcal{H})t\right]Q(\gamma,t), \qquad (A16)$$

$$Q(\gamma,t) = \exp\left[-D_x t\left(\gamma^2 + \frac{iU}{D_x}\gamma\right)\right]. \qquad (A17)$$

In view of eqns (A12) and (A14), and application of the convolution theorem, the inverse Laplace transformation of eqn (A7) with respect to s is given by

$$\bar{\hat{\bar{C}}}(t,\gamma,\omega,z) = \frac{1}{2D_z}\int_{0}^{t}\int_{0}^{\infty}\bar{\hat{\bar{F}}}(t-\tau,\gamma,\omega,p)\Bigg[\mathcal{H}\bar{\hat{\bar{P}}}(\tau,\gamma,\omega,z+p)$$
$$+\frac{\partial \bar{\hat{\bar{P}}}(\tau,\gamma,\omega,z+p)}{\partial\tau} + \mathcal{H}\bar{\hat{\bar{P}}}(\tau,\gamma,\omega,p-z)$$
$$+\frac{\partial \bar{\hat{\bar{P}}}(\tau,\gamma,\omega,p-z)}{\partial\tau}\Bigg]\,dp\,d\tau. \qquad (A18)$$

The inverse Fourier transformation of eqn (A18) with respect to γ is

$$\bar{C}(t,x,\omega,z) = \left(\frac{1}{8\pi D_z^2}\right)^{1/2}\int_{0}^{t}\int_{-\infty}^{\infty}\int_{0}^{\infty}\bar{F}(t-\tau,q,\omega,p)$$
$$\times \Bigg[\mathcal{H}\bar{P}(\tau,x-q,\omega,z+p)$$
$$+\frac{\partial \bar{P}(\tau,x-q,\omega,z+p)}{\partial\tau}$$
$$+\mathcal{H}\bar{P}(\tau,x-q,\omega,p-z)$$
$$+\frac{\partial \bar{P}(\tau,x-q,\omega,p-z)}{\partial\tau}\Bigg]\,dp\,dq\,d\tau, \quad (A19)$$

where the following definitions of the Fourier inverse transform were employed:

$$\mathcal{F}^{-1}\{\hat{f}_1(\gamma)\} = \frac{1}{(2\pi)^{1/2}} \int_{-\infty}^{\infty} \hat{f}_1(\gamma) e^{i\gamma x}\, d\gamma, \qquad (A20)$$

$$\mathcal{F}^{-1}\{\hat{f}_1(\gamma)\hat{f}_2(\gamma)\} = \frac{1}{(2\pi)^{1/2}} \int_{-\infty}^{\infty} f_1(x-\xi)f_2(\xi)\, d\xi, \qquad (A21)$$

where $\mathcal{F}^{-1}$ is the Fourier inverse operator and ξ is a dummy integration variable.

In order to obtain the inverse Fourier transformation of eqn (A15) with respect to γ, only the term $Q(\gamma,t)$ defined in eqn (A17) requires inversion, and is obtained as follows:

$$\mathcal{F}^{-1}\{Q(\gamma,t)\} = \frac{1}{(2\pi)^{1/2}} \int_{-\infty}^{\infty} \exp\left[-D_x t\left(\gamma^2 + \frac{iU}{D_x}\gamma\right)\right]$$
$$\times e^{i\gamma x}\, d\gamma = \left(\frac{1}{2D_x t}\right)^{1/2} \eta(x,t), \qquad (A22)$$

where

$$\eta(x,t) = \exp\left[-\frac{1}{D_x}\left(\frac{U^2 t}{4} + \frac{x^2}{4t} - \frac{Ux}{2}\right)\right], \qquad (A23)$$

and the latter expression in eqn (A22) is a consequence of employing Euler's formula ($e^{i\gamma x} = \cos(\gamma x) + i\sin(\gamma x)$) and the integral identities found in Gradshteyn and Ryzhik[9] (eqn 3.923.1 and 2, p. 485) were utilized. Therefore, in view of eqn (A22), the inverse Fourier transformation of eqn (A15) is

$$\bar{\mathcal{P}}(t,x,\omega,z) = e^{-\mathcal{H}t} \int_0^t I_0\left[2\left(\mathcal{B}\zeta(t-\zeta)\right)^{1/2}\right]\left(\frac{D_z}{2\pi D_x \zeta^2}\right)^{1/2}$$
$$\times \exp\left[-\frac{z^2}{4D_z\zeta} - \left(\omega^2 D_y + \mathcal{A} - \mathcal{H}\right)\zeta\right]$$
$$\times \eta(x,\zeta)\, d\zeta. \qquad (A24)$$

The inverse Fourier transformation of eqn (A19) with respect to ω is

$$C(t,x,y,z) = \frac{1}{4\pi D_z} \int_0^t \int_{-\infty}^{\infty} \int_{-\infty}^{\infty} \int_0^{\infty} F(t-\tau,q,v,p)$$
$$\times \Bigg[\mathcal{H}\mathcal{P}(\tau,x-q,y-v,z+p)$$
$$+ \frac{\partial\mathcal{P}(\tau,x-q,y-v,z+p)}{\partial\tau}$$
$$+ \mathcal{H}\mathcal{P}(\tau,x-q,y-v,p-z)$$
$$+ \frac{\partial\mathcal{P}(\tau,x-q,y-v,p-z)}{\partial\tau}\Bigg]\, dp\, dv\, dq\, d\tau. \qquad (A25)$$

In view of the following inverse Fourier transform relationship (see Kreryszig,[13] eqn 9, p. 621):

$$\mathcal{F}^{-1}\{\exp[-\omega^2 D_y \zeta]\} = \left(\frac{1}{2D_y\zeta}\right)^{1/2}\exp\left[-\frac{y^2}{4D_y\zeta}\right], \qquad (A26)$$

the inverse Fourier transformation of eqn (A24) is

$$\mathcal{P}(t,x,y,z) = e^{-\mathcal{H}t} \int_0^t I_0\left[2\left(\mathcal{B}\zeta(t-\zeta)\right)^{1/2}\right]\left(\frac{D_z}{4\pi D_x D_y \zeta^3}\right)^{1/2}$$
$$\times \exp\left[-\frac{z^2}{4D_z\zeta} - \frac{y^2}{4D_y\zeta} - (\mathcal{A}-\mathcal{H})\zeta\right]$$
$$\times \eta(x,\zeta)\, d\zeta. \qquad (A27)$$

Furthermore, in order to complete the description of eqn (A25), the derivative of $\mathcal{P}(t,x,y,z)$ with respect to t is obtained as follows:

$$\frac{\partial\mathcal{P}(t,x,y,z)}{\partial t} = e^{-\mathcal{H}t} \int_0^t \left\{\left(\frac{\mathcal{B}\zeta}{t-\zeta}\right)^{1/2} I_1\left[2\left(\mathcal{B}\zeta(t-\zeta)\right)^{1/2}\right]\right.$$
$$\left. - \mathcal{H}I_0\left[2\left(\mathcal{B}\zeta(t-\zeta)\right)^{1/2}\right]\right\}$$
$$\times \left(\frac{D_z}{4\pi D_x D_y \zeta^3}\right)^{1/2}$$
$$\times \exp\left[-\frac{z^2}{4D_z\zeta} - \frac{y^2}{4D_y\zeta} - (\mathcal{A}-\mathcal{H})\zeta\right]$$
$$\times \eta(x,\zeta)\, d\zeta + e^{-\mathcal{H}t}\left(\frac{D_z}{4\pi D_x D_y t^3}\right)^{1/2}$$
$$\times \exp\left[-\frac{z^2}{4D_z t} - \frac{y^2}{4D_y t} - (\mathcal{A}-\mathcal{H})t\right]\eta(x,t). \qquad (A28)$$

Substituting eqn (A23) into eqns (A27) and (A28) and subsequently substituting the resulting expressions into eqn (A25) yields the desired generalized analytical solution, eqns (16), (17a)–(17d).

APPENDIX B DERIVATION OF THE ANALYTICAL SOLUTION FOR AN AQUIFER WITH FINITE THICKNESS

The analytical solution for the case of an aquifer with finite thickness is obtained by solving eqn (4) subject to eqns (11)–(14) and (28). Taking the Laplace transform with respect to the time variable t, Fourier transforms with respect to space variables x and y, and the finite Fourier cosine transform with respect to space variable z of eqn (4) and subsequently employing transformed initial condition (11) yields

$$\bar{\bar{\bar{C}}}(s,\gamma,\omega,\psi_m) = \frac{\bar{\bar{\bar{F}}}(s,\gamma,\omega,\psi_m)}{\gamma^2 D_x + i\gamma U + E}, \qquad (B1)$$

where

$$E = \omega^2 D_y + \psi_m^2 D_z + \mathcal{A} + s - \frac{\mathcal{B}}{s+\mathcal{H}}, \qquad (B2)$$

the Laplace and Fourier transformation properties (A3)–(A5), and the following finite Fourier cosine transformation and

operational property were employed (see Churchill,[6] p. 294):

$$\ddot{\bar{\tilde{C}}}(s,\gamma,\omega,\psi_m) = \int_0^H \bar{\tilde{C}}(s,\gamma,\omega,z)\cos(\psi_m z)\,\mathrm{d}z, \qquad (B3)$$

$$\mathcal{F}_{\mathrm{fc}}\left\{\frac{\mathrm{d}^2 f(z)}{\mathrm{d}z^2}\right\} = \psi_m^2 \ddot{f}(\psi_m^2) - \frac{\mathrm{d}f(0)}{\mathrm{d}z}$$
$$+ (-1)^m \frac{\mathrm{d}\ddot{f}(H)}{\mathrm{d}z} \quad (m=0,1,2\ldots), \quad (B4)$$

where the double over-dot signifies finite Fourier cosine transform with respect to space variable z, with corresponding finite Fourier cosine transform variable $\psi_m = m\pi/H$, $\mathcal{F}_{\mathrm{fc}}$ is the finite Fourier cosine transform operator and f is an arbitrary function.

The Fourier inverse transformation of eqn (B1) with respect to γ is obtained by employing the Fourier inverse transforms (A20) and (A21), Euler's formula, integral identities found in Gradshteyn and Ryzhik[9] (eqns 3.724.1 and 2, p. 407), eqn (B2) and application of the convolution theorem as follows:

$$\ddot{\bar{\tilde{C}}}(s,x,\omega,\psi_m) = \int_{-\infty}^\infty \ddot{\bar{\tilde{F}}}(s,q,\omega,\psi_m)\Psi(s,x-q,\omega,\psi_m)\,\mathrm{d}q, \qquad (B5)$$

where

$$\Psi(s,x,\omega,\psi_m) = \left(\frac{1}{4D_xD_y(\omega^2+\mathcal{S})}\right)^{1/2}\exp\left[\frac{Ux}{2D_x}\right]$$
$$\times \exp\left[-x\left((\omega^2+\mathcal{S})\frac{D_y}{D_x}\right)^{1/2}\right], \qquad (B6)$$

$$\mathcal{S} = \frac{1}{D_y}\left(\psi_m^2 D_z + \mathcal{A} + s - \frac{\mathcal{B}}{s+\mathcal{H}} + \frac{U^2}{4D_x}\right). \qquad (B7)$$

In view of eqns (A20), (A21) and (B6), Euler's formula, the integral identity found in Gradshteyn and Ryzhik[9] (eqn 3.961.2, p. 498), and application of the convolution theorem, the inverse Fourier transformation of eqn (B5) with respect to ω is given by

$$\ddot{\bar{C}}(s,x,y,\psi_m) = \int_{-\infty}^\infty \int_{-\infty}^\infty \ddot{\bar{F}}(s,q,v,\psi_m)g(s,x-q,y-v,\psi_m)\,\mathrm{d}v\,\mathrm{d}q, \qquad (B8)$$

where

$$g(s,x,y,\psi_m) = \left(\frac{1}{4\pi^2 D_x D_y}\right)^{1/2}\exp\left[\frac{Ux}{2D_x}\right]$$
$$\times K_0\left[\mathcal{S}^{1/2}\left(y^2 + x^2\frac{D_y}{D_x}\right)^{1/2}\right]. \qquad (B9)$$

In view of eqns (B7) and (B9), the inverse Laplace transform (see Roberts and Kaufman,[17] eqn 3, p. 169 and eqn 13.2.1, p. 304):

$$f_0(t) = \mathcal{L}^{-1}\left\{K_0\left[\beta_1(s+\beta_2)^{1/2}\right]\right\} = \frac{1}{2t}\exp\left[\frac{-\beta_1^2}{4t} - \beta_2 t\right], \qquad (B10)$$

and by following the procedures outlined in Appendix A, the inverse Laplace transformation of eqn (B8) with respect to s is given by

$$\ddot{C}(t,x,y,\psi_m) = \left(\frac{1}{16\pi^2 D_x D_y}\right)^{1/2}\int_0^t\int_{-\infty}^\infty\int_{-\infty}^\infty$$
$$\times \exp\left[\frac{U(x-q)}{2D_x}\right]e^{-\mathcal{H}\tau}\ddot{F}(t-\tau,q,v,\psi_m)$$
$$\times \left\{\int_0^\tau \left(\frac{\mathcal{B}}{\zeta(\tau-\zeta)}\right)^{1/2} I_1\left[2(\mathcal{B}\zeta(\tau-\zeta))^{1/2}\right]\right.$$
$$\times \exp\left[-\zeta\left(\psi_m^2 D_z + \mathcal{A} + \frac{U^2}{4D_x} - \mathcal{H}\right)\right]$$
$$\times \exp\left[-\frac{1}{4\zeta}\left(\frac{(x-q)^2}{D_x} + \frac{(y-v)^2}{D_y}\right)\right]\mathrm{d}\zeta$$
$$+ \frac{1}{\tau}\exp\left[-\tau\left(\psi_m^2 D_z + \mathcal{A} + \frac{U^2}{4D_x} - \mathcal{H}\right)\right]$$
$$\times \exp\left[-\frac{1}{4\tau}\left(\frac{(x-q)^2}{D_x} + \frac{(y-v)^2}{D_y}\right)\right]\right\}$$
$$\times \mathrm{d}v\,\mathrm{d}q\,\mathrm{d}\tau. \qquad (B11)$$

The inverse Fourier cosine transformation of eqn (B11) with respect to ψ_m is given by

$$C(t,x,y,z) = \left(\frac{1}{16\pi^2 D_x D_y}\right)^{1/2}\int_0^t\int_{-\infty}^\infty\int_{-\infty}^\infty$$
$$\times \exp\left[\frac{U(x-q)}{2D_x}\right]e^{-\mathcal{H}\tau}$$
$$\times \left\{\int_0^\tau \left(\frac{\mathcal{B}}{\zeta(\tau-\zeta)}\right)^{1/2} I_1\left[2(\mathcal{B}\zeta(\tau-\zeta))^{1/2}\right]\right.$$
$$\times \exp\left[-\frac{1}{4\zeta}\left(\frac{(x-q)^2}{D_x} + \frac{(y-v)^2}{D_y}\right)\right]$$
$$\times \exp\left[-\zeta\left(\mathcal{A} + \frac{U^2}{4D_x} - \mathcal{H}\right)\right]$$
$$\times \mathcal{F}_{\mathrm{fc}}^{-1}\left\{\ddot{F}(t-\tau,q,v,\psi_m)\exp\left[-\psi_m^2 D_z\zeta\right]\right\}\mathrm{d}\zeta$$
$$+ \frac{1}{\tau}\exp\left[-\frac{1}{4\tau}\left(\frac{(x-q)^2}{D_x} + \frac{(y-v)^2}{D_y}\right)\right]$$
$$\times \exp\left[-\tau\left(\mathcal{A} + \frac{U^2}{4D_x} - \mathcal{H}\right)\right]$$
$$\times \mathcal{F}_{\mathrm{fc}}^{-1}\left\{\ddot{F}(t-\tau,q,v,\psi_m)\exp\left[-\psi_m^2 D_z\tau\right]\right\}\right\}$$
$$\times \mathrm{d}v\,\mathrm{d}q\,\mathrm{d}\tau, \qquad (B12)$$

where $\mathcal{F}_{\mathrm{fc}}^{-1}$ is the inverse finite Fourier cosine operator, defined as

$$\mathcal{F}_{\mathrm{fc}}^{-1}\{\ddot{f}(\psi_m)\} = \frac{\ddot{f}(0)}{H} + \frac{2}{H}\sum_{m=1}^\infty \ddot{f}(\psi_m)\cos(\psi_m z), \ 0 \le z \le H. \qquad (B13)$$

In view of eqn (B13), eqn (B12) is simplified to the form of the generalized analytical solution, eqns (29)–(31).